PNAS

Supporting Information for

Identification and targeting of a unique $Na_V1.7$ domain driving chronic pain

Kimberly Gomez[1,2,a], Harrison J. Stratton[3,a], Paz Duran[1,2], Santiago Loya[1,2], Cheng Tang[1,2], Aida Calderon-Rivera[1,2], Liberty François-Moutal[3], May Khanna[1,2], Cynthia L. Madura[3], Shizhen Luo[3], Bryan McKiver[5], Edward Choi[5], Dongzhi Ran[3], Lisa Boinon[3], Samantha Perez-Miller[1,2], M. Imad Damaj[5], Aubin Moutal[4, †], and Rajesh Khanna[1,2,6,†,*]

Affiliations:

[1]Department of Molecular Pathobiology, College of Dentistry, New York University, New York, NY, 10010, USA.

[2]NYU Pain Research Center, 433 1st Avenue Room 822 New York, NY 10010, USA.

[3]Department of Pharmacology, College of Medicine, The University of Arizona, Tucson, AZ, 85724 USA.

[4]Department of Pharmacology and Physiology, School of Medicine, St. Louis University, St. Louis, MO, 63104, USA.

[5]Department of Pharmacology and Toxicology and Translational Research Initiative for Pain and Neuropathy, Virginia Commonwealth University, USA

[6]Department of Neuroscience and Physiology and Neuroscience Institute, School of Medicine, New York University, New York, NY, 10010, USA.

[a]Co-first authors

[†]Contributed equally to this work

[*]To whom correspondence should be addressed:

Dr. Rajesh Khanna, Department of Molecular Pathobiology, College of Dentistry, New York University, 433 1st Avenue Room 822 New York, NY 10010, USA. Email: rk4272@nyu.edu ORCID #: 0000-0002-9066-2969

This PDF file includes:

SI Materials and Methods

Figures S1 to S10

Tables S1 to S4

SI References

Supporting Information

SI Materials and Methods

Study Design. This study was designed with the aim of elucidating the mechanism of CRMP2 dependent regulation of $Na_V1.7$ in the context of chronic pain. We approached this question from the standpoint of translating our findings to human therapies and to this end we made the decision to include the human $Na_V1.7$ channel as often as was feasible. To identify the interaction domain between CRMP2 and human $Na_V1.7$ we printed the cytoplasmic loops of the channel on a peptide array. We probed this array with lysates from three species to ensure our findings were the same across species. We used biochemical approaches to validate the interaction in cultured cells and investigated the effects of disrupting this interaction on $Na_V1.7$ trafficking and CRMP2 post-translational modifications. We then sought to identify the electrophysiological consequences of disrupting this interaction using DRG neurons transfected with a mutant $Na_V1.7$ encoding plasmid or treated with an interfering peptide. Furthermore, we investigated the effects of our disruption strategy in multiple different pain models to assay the off-target and on-target actions of this approach.

Animals. Adult male and female Sprague-Dawley rats (Pathogen-free male and female 100–250 g, Envigo, Placentia, CA) and male and female mice (C57BL/6NHsd, 20–24 g; Envigo) were kept in light (12-h light: 12-h dark cycle; lights on at 07:00 h) and temperature (23 ± 3°C) controlled rooms. Standard rodent chow and water were available *ad libitum.* All animal use was conducted in accordance with the National Institutes of Health guidelines, and the study was conducted in strict accordance with recommendations in the Guide for the Care and Use of Laboratory Animals of the University of Arizona (Protocol #: 16-141). Two adult male macaques (*Macaca mulatta*), aged 7 and 11 years, were used in this study. All animals were housed and bred in the University of Arizona Laboratory Animal Research Center. The same animals were tested using no more than 2 noninvasive behavioral assessments to reduce the number of mice and rats needed to complete the study.

For the paclitaxel experiments, a total of 32 adult male and female (50% male and 50% female for each group- (n = 8/group) C57BL/6J (8–10 weeks of age at the beginning of experiments; The Jackson Laboratory; JAX - Bar Harbor, ME USA), were used in the study. Mice were randomly chosen and assigned to treatment groups and groups were blinded to the experimenters. Male and female animals were used in each experiment and groups were equally balanced such that each experiment contained mixed-sex cohorts. Mice were housed in a temperature- (21°C) and humidity-controlled Association for Assessment and Accreditation of Laboratory Animal Care-approved animal care facility at Virginia Commonwealth University on a 12-hour light/dark cycle (lights on at 7:00 AM). Mice were housed in groups of four with Teklad corn cob bedding (#7097, Envigo Teklad, Madison, WI, USA), and received free access to food (#7012, Teklad LM-485 mouse sterilized diet, Envigo, Madison, WI) and water. They also received enrichment consisting of shreddable 5 x 5cm nesting materials (Nestlets™, Avantor Inc., Radnor Township, PA) per cage made of sterilized pulped virgin cotton fiber, along with a red Safe Harbor Mouse Retreat™ hut (Bio-Serv, Flemington, NJ). All experiments were performed during the light cycle, and the study was approved by the Institutional Animal Care and Use Committee of Virginia Commonwealth University. All studies were carried out in accordance with the National Institutes of Health's Guide for the Care and Use of Laboratory Animals. All efforts were made to minimize animal suffering. All behavioral experiments were performed by experimenters who were blinded to the genotype, and sex, and treatment groups.

Materials and Reagents. Peptides with the TAT cell penetrating sequence, YGRKKRRQRRR, fused to the CRMP2 binding domain of $Na_V1.7$, SRGKCPPWWYRFAHK, were synthesized and HPLC-purified (>95% purity) by Genscript Inc. (Piscataway, NJ, USA). Scramble and random sequence-based peptides

conjugated to various cargoes as controls have been previously studied as controls in molecular, biochemical, and behavioral assays and demonstrated to have no effects (1-4).

Peptide SPOT Array. Peptide spot arrays (15-mers with an overlap of 12 residues) spanning intracellular loops of human $Na_V1.7$ were constructed using the SPOTS-synthesis method. Standard 9-fluorenylmethoxy carbonyl (Fmoc) chemistry was used to synthesize the peptides and spot them onto nitrocellulose membranes pre-derivatized with a polyethylene glycerol spacer (Intavis AG). Fmoc-protected and Fmoc-activated amino acids were spotted in 20 by 30 arrays on 150 mm by 100-mm membranes using an Intavis MultiPep robot. The nitrocellulose membrane containing the immobilized peptides was soaked in N-cyclohexyl-3-aminopropanesulfonic acid (CAPS) buffer (10 mM CAPS, pH 11.0 with 20% vol/vol methanol) for 30 minutes, washed once with Tris-buffered 0.1% Tween 20 (TBST), and then blocked for 1 hour at room temperature (RT) with gentle shaking in TBST containing 5% (mass/vol) nonfat milk and then incubated with rat, pig, and human spinal cord protein for 1 hour at RT with gentle shaking. Next, the membranes were incubated in primary antibody for CRMP2 for 2 hours at RT with gentle shaking, followed by washing with TBST. Finally, the membranes were incubated in secondary antibody (goat anti-rabbit DyLight 800, Cat# 355571, Thermo Fisher) for 45 minutes, washed for 30 minutes in TBST and visualized by infrared fluorescence (Li-Cor Odyssey Clx Imaging System; LI-COR Biosciences, Lincoln, NE). 2-4 independent peptide spot arrays were used in this study.

Determination of Myr-TAT-Nav1.7-CRS peptide in rat CSF. The stability of Myr-TAT-Nav1.7-CRS peptide in rat CSF was determined by WuXi Apptec (Lab Testing Division, Cranbury NJ, USA). Male pooled Sprague Dawley rat CSF was obtained from BIOIVT (Catalog # RAT00CSF-0001022 and lot # RAT538976). A final concentration of 2 µM Myr-TAT-Nav1.7-CRS peptide from a stock of 5 mM in DMSO was used for these experiments. Briefly, prior to the start of the experiment, the pooled frozen SD Rat CSF was thawed in a water bath at 37ºC. 20µl of the TA working solution (40µM) was added into two 2.0 ml low binding tubes. 380µl of the warm SD Rat CSF was added to each tube and mixed well. From each tube, 50µl of the sample was taken for T0 sample, which was then mixed with stop solution (10ng/ml Tolbutamide/Labetalol hydrochloride in MeOH:H2O(3:7) with 1% FA). At each time point (10, 30, 60, and 120 minutes), 50µl of sample from each tube was taken and transferred into a low binding 96-well plate and quenched with 10ng/ml Tolbutamide/Labetalol hydrochloride in MeOH:H2O(3:7) with 1% FA. The sample plate was submitted for LC/MS/MS analysis.

Preparation of spinal cord lysates. Lumbar segment of spinal cord lysates prepared from adult Sprague-Dawley rats were generated by homogenization and sonication in lysis buffer (50 mM Tris-HCl, pH 7.4, 50 mM NaCl, 2 mM $MgCl_2$, 1% [vol/vol] NP40, 0.5% [mass/vol] sodium deoxycholate, 0.1% [mass/vol] sodium dodecyl sulfate [SDS]) as previously described (5). The lysis buffer included freshly added protease inhibitors (Cat# B14002; Biotools, Houston, TX), phosphatase inhibitors (Cat# B15002, Biotools), and Benzonase (Cat# 71206; Millipore, Billerica, MA). Protein concentrations were determined using the bicinchoninic acid protein assay (Cat# PI23225, Thermo scientific).

Structural modeling and computational methods. Secondary structure prediction was conducted using PSIPRED (6). Initially, the full 315 amino acid intracellular domain of $Na_V1.7$ was submitted to SwissModel (7), Phyre2 intensive mode (8) and I-TASSER (9). SwissModel and Phyre2 returned homology models only for the peptide in the region covering amino acids 708-724 and 706-720, respectively, both consistent with a predominantly alpha helical structure. I-TASSER returned only low-quality models for the intracellular domain with the top results also consistent with a helical structure for the peptide. Subsequently, all 9 NaV isoform peptides were submitted to I-TASSER with their respective 6 flanking amino acids included at both ends (the equivalent of $Na_V1.7$ amino acids 700-726), due to minimum size for prediction. The resultant models all exhibited a loop-helix for the equivalent of residues 706-720 with C-scores in the range of -1.82 to -0.64, estimated TM-scores from 0.49 to 0.63, and estimated RMSDs from 2.7 – 5.0 Å.

Microscale Thermophoresis (MST). MST is an assay that measures the thermophoretic movement of molecules in optically generated microscopic temperature gradients allowing analysis of biomolecular interactions (10). In MST, increasing concentrations of unlabeled ligand are mixed with the fluorescently labeled biomolecule which is kept at a constant concentration. Purified CRMP2-His was fluorescently labelled with a His-Tag labeling kit RED-Tris-NTA (Nanotemper, Germany) per manufacturer's instructions. Two hundred nanomolar of CRMP2-His (in PBS supplemented with 0.05% Tween-20 (PBS-T

buffer)) was mixed with 1M NT-647-His-labeling dye. After incubating for 30 min at room temperature, labeled CRMP2 was pelleted by centrifugation at 15,000 x (g) for 10 min at 4°C. 50 nM of NTA-labeled His-CRMP2 was mixed with varying concentrations of the $Na_V1.7$-CRS (SRQKCPPWWYRFAHK) or the analogous region from all other voltage gated sodium channels (NaV1.X) in PBS-T and incubated at room temperature for 10 min. The thermophoresis readouts were captured on a Monolith NT.115 (Nanotemper, Germany) using premium MST capillaries, at 40% LED and 40% MST power. Data analysis was performed with the MO Affinity Analysis software (Nanotemper) using the Kd model (standard fitting model derived from law of mass action).

Catecholamine A Differentiated (CAD) Cell Culture. Mouse neuron derived Cathecholamine A differentiated CAD cells (ECACC cat. no. 08100805, RRID: CVCL_0199) were grown in standard cell culture conditions, 37 °C in 5% (vol/vol) CO2. They were maintained in DMEM/F12 media supplemented with 10% (vol/vol) FBS (HyClone) and 1% penicillin/streptomycin sulfate from 10,000 µg/mL stock.

Co-immunoprecipitation. CAD cells were lysed into the IP buffer containing: 20 mM Tris·HCl, pH 7.4, 50 mM NaCl, 2 mM $MgCl_2$, 10 mM N-ethylmaleimide, 1% (vol/vol) Igepal CA-630, 0.5% (mass/vol) sodium deoxycholate, 0.1% (mass/vol) SDS with protease inhibitors (cat. no. B14002; Biotool), and phosphatase inhibitors (cat. no. B15002, Biotool). Total protein concentration was determined using a bicinchoninic acid (BCA) assay (cat. no. PI23225; Thermo Fisher Scientific), and then 500 µg of total protein was incubated with 3 µg of CRMP2 antibody overnight at 4 °C under gentle agitation.
For Co-IP of endogenously SUMOylated proteins, 0.5% SDS was added to the lysates at 0.5% (mass/vol) final concentration, before boiling for 5 min at 95 °C. Then, 500 µg of total proteins were incubated with 5 µg of SUMO1 antibody overnight at 4 °C under gentle agitation. Protein G magnetic beads (cat. no. 10009D; Thermo Fisher Scientific), preequilibrated with the IP buffer, were then added to the lysates and incubated for 1 h at 4 °C to capture immunocomplexes. Beads were washed four times with IP buffer to remove nonspecific binding of proteins before resuspension in Laemmli buffer and boiling at 95 °C for 5 min before immunoblotting.

Identification of endogenous CRMP2 SUMOylation is challenging due to the presence of basal isopeptidase activity. To overcome this issue, we prepared CAD cell lysates in a denaturing buffer, followed by heat denaturing to inactivate SUMO isopeptidases and completely unfold the protein, which eliminates non-covalent SUMO1 interactions (11). We then performed immunoprecipitation with a SUMO1 antibody followed by western blot to detect SUMOylated CRMP2.

CRMP2-HIS pull-down. HIS tag Dynabeads (Cat# 10103D, Invitrogen), preincubated with purified CRMP2-HIS (0.5 µM), were incubated overnight with 300 µg of total protein from macaque spinal cord lysates at 4 ºC in the presence of the indicated peptides (5 µM) with gentle rotation. Beads were washed 3 times with lysis buffer before resuspension in Laemmli buffer and denaturation (5 minutes at 95 ºC) and immunoblotting as described previously.

Cell-surface biotinylation. Biotinylation was performed as described previously (1, 12). Briefly, live CAD cells were incubated with 0.5 mg·mL−1 sulfosuccinimidyl 6-(biotin-amido) hexanoate (EZ-Link Sulfo-NHS-LC-Biotin; cat. no. 21335; Thermo Fisher Scientific) for 30 min at 4 °C in cold PBS solution. Excess biotin was quenched by three washes with ice-cold PBS solution containing 100 mM glycine then washed three times with ice-cold PBS solution. The cells were lysed in lysis buffer containing: 20 mM Tris·HCl, pH 7.4, 50 mM NaCl, 2 mM $MgCl_2$, 1% (vol/vol) Igepal CA-630 (cat. No. 19628; USBiological Life Sciences), 0.5% (mass/vol) sodium deoxycholate with protease inhibitors (cat. no. B14002; Biotool), and phosphatase inhibitors (cat. no. B15002; Biotool)]. The biotinylated proteins were separated by adsorption onto Dynabeads M-280 Streptavidin (cat. no. 11205D; Thermo Fisher Scientific) overnight at 4 °C. Beads were washed three times with lysis buffer, resuspended in Laemmli buffer, and heated at 95 °C for 5 min before immunoblotting.

Immunoblotting. Indicated samples were loaded on 4–20% Novex gels (cat. no. XP04205BOX; Thermo Fisher Scientific). Proteins were transferred for 1 h at 120 V using TGS [25 mM Tris, pH 8.5, 192 mM glycine, 0.1% (mass/vol) SDS], with 20% (vol/vol) methanol as transfer buffer to PVDF membranes (0.45 µm; cat. no. IPFL00010; Millipore), preactivated in pure methanol. After transfer, the membranes were blocked at room temperature for 1 h with TBST (50 mM Tris·HCl, pH 7.4, 150 mM NaCl, 0.1% Tween 20) with 5% (mass/vol) nonfat dry milk, and then incubated separately with the following primary antibodies

diluted in TBST, 5% (mass/vol) BSA, overnight at 4 °C: $Na_V1.7$ (cat. no. ab85015; Abcam), βIII-Tubulin (cat. no. G7121; Promega), CRMP2 (cat. no. C2993; Sigma-Aldrich), SUMO1 (cat. no. S8070; Sigma-Aldrich), $Ca_V2.2$ (cat. no. TA308673; Origene), Na^+/K^+ ATPase a-1 (cat. no. 05-369-25UG; Sigma-Aldrich), PSD-95 (cat. no. MA1-045; Invitrogen), Synaptophysin (cat. no. MAB5258; Sigma-Aldrich), CRMP2 pSer522 (cat. no. CP2191; ECM Biosciences) and CRMP2 pThr514 (cat. no. PA5-110113; Invitrogen). Next, the membranes were incubated in HRP-conjugated secondary antibodies from Jackson ImmunoResearch, and blots were developed by enhanced luminescence (WBKLS0500; Millipore) before exposure to photographic film.

Calcitonin gene-related peptide (CGRP) release assay. Rats were anesthetized with 5% isofluorane and then decapitated. Two vertebral incisions (cervical and lumbar) were made to expose the spinal cord. Pressure was applied to a saline-filled syringe inserted into the lumbar vertebral foramen, and the spinal cord was extracted. Only the lumbar region of the spinal cord was used for the CGRP release assay. Baseline treatments (#1 and #2) involved bathing the spinal cord in standard Tyrode solution. The excitatory solution, consisting of 90 mM KCl, was paired with the treatment for fraction #4. These fractions (5 minutes, 700 µL each) were collected for measurement of CGRP release. Samples were immediately stored in a −20˚C freezer. Myr-TAT-$Na_V1.7$-CRS (5 µM), Myr-TAT-SCR, or vehicle (0.9% saline) was added to the pretreatment and cotreatment fractions (#3 and 4). The concentration of CGRP released into the buffer was measured by enzyme-linked immunosorbent assay (Cat# 589001; Cayman Chemical, Ann Arbor, MI).

Synaptic fractionation and enrichment. Adult rats were anesthetized using isoflurane and decapitated. Spinal cords were removed, and the dorsal horn of the spinal cord was dissected as this structure contains the synapses arising from the DRG. Synaptosomes isolation was done as described previously (13). Integrity of non-postsynaptic density (non-PSD) and PSD fractions was verified by immunoblotting. PSD95 was enriched in the PSD fractions while synaptophysin was enriched in non-PSD fractions. BCA protein assay was used to determine protein concentrations.

Acute dissociation, culture, and transfection of dorsal root ganglia (DRG) neurons. Dorsal root ganglia (DRG) were dissected from 100 g female Sprague-Dawley rats employing procedures described previously (14). For non-transfected cells, dissociated DRG neurons were plated onto 12 mm poly-D-lysine and laminin-coated glass coverslips and cultured for up to 24-48 h. For siRNA-Control and siRNA-CRMP2 transfection, collected cells were resuspended in Nucleofector transfection reagent containing siRNAs at a working concentration of 600 nM. Then, cells were subjected to electroporation protocol O-003 in an Amaxa Biosystem (Lonza), plated onto 12-mm poly-D-lysine- and laminin-coated glass coverslips and cultured for up to 48-72 h. siRNA transfection was verified by GFP fluorescence. Transfection efficiencies were between 20% and 30%, with approximately 10% cell death. For experiments with the Halo-$Na_V1.7$ channels cells were transfected with 8µg of DNA before resuspension and plating onto glass coverslips. In experiments with the AAV plasmid encoding the $Na_V1.7$ peptide or the scrambled control cells were mixed with 6 µg of DNA before transfection and plating.

Calcium Imaging. Changes in depolarization-induced calcium influx in rat DRG neurons were determined with Fura-2AM as previously described (3, 15). DRG neurons were incubated with 5 µM of Myr-TAT-peptides or DMSO as control, for a duration of 30 min. A standard bath solution containing 139 mM NaCl, 3 mM KCl, 0.8 mM $MgCl_2$, 1.8 mM $CaCl_2$, 10 mM Na-HEPES, pH 7.4, 5 mM glucose was used. Depolarization was evoked with a 10 sec pulse of 90 mM KCl.

HaloTag and Halo-Nav1.7 current isolation. To Identify and characterize the effect of swapping the $Na_V1.7$-CRS with analogous sequences from all other voltage-gated sodium channels we adapted a modified volage gated sodium channel construct originally developed in Waxman Laboratory. The construct was composed of the alpha subunit of the volage gated sodium channel $Na_V1.7$ with a β4 subunit fused to the N-terminus of the alpha subunit. The extracellular immunoglobulin-like domain of the β4 subunit was replaced with the HaloTag reporter enzyme. This substitution with the HaloTag reporter enzyme meant that when the after the addition of the Halo Ligand to the external solution, all cells that were successfully transfected would fluoresce in the green spectrum. The final construct had the following

topology from the N-terminus: amino acids 1-30 β4 signal peptide; Three Myc tags (EQKLISEEDL), HaloTag enzyme (297 amino acids), Three HA tags (YPYDVPDYA), β4 transmembrane segment (β4 residues 163-183), linker sequence (SGLRSAT), $Na_V1.7$ alpha subunit. Importantly, this plasmid contains a mutation, Tyr-362 to Ser (Y362S), that confers resistance to the voltage gated sodium channel blocker tetrodotoxin (TTX) (16, 17).

In the Halo-Nav1.7 experiments, we record with TTX in the solution to inactivate all endogenous TTX-S currents. While the channel encoded by this plasmid is pharmacologically resistant to TTX, it retains the biophysical properties of $Na_V1.7$. This is important because adult rat DRG neurons express tetrodotoxin-sensitive (TTX-S; mainly $Na_V1.1$, $Na_V1.6$ and $Na_V1.7$) and tetrodotoxin-resistant (TTX-R; NaV1.8 and 1.9) voltage-gated sodium channels (18, 19). The kinetics of activation and inactivation of these channels are widely accepted to be different, with TTX-S channels exhibiting fast inactivation, and TTX-R channels displaying slower kinetics (20). We leverage the differences in biophysical properties of these channel populations to dissect TTX-R currents from TTX-S currents, which has been shown to be equivalent to pharmacological separation (21). This process is based on the approach we have previously published in Dustrude et al 2016. To perform this isolation, we execute a steady state availability protocol (like Zhang et al, 2017). To measure the total current, we apply conditioning pre pulses, from -120 mV to +10 mV, to inactivate a portion of sodium channels before a test pulse to 0 mV is applied (Fig 1F). The test pulse current after the conditioning pre pulse to -40 mV, which represents the TTX-R current, is then subtracted from the total current (Fig 1G, pink trace). This yields the Halo-NaV1.7 current fraction. Using this approach, we can isolate currents with TTX-R kinetics from currents with TTX-S inactivation kinetics.

Whole-cell voltage clamp electrophysiology. Patch-clamp recordings were performed at room temperature (22–24°C). Currents were recorded using an EPC 10 Amplifier-HEKA linked to a computer with Patchmaster software. 5 μM of Myr-TAT-SCR and Myr-TAT-$Na_V1.7$-CRS peptides and 10 μM of TAT-SCR and TAT-$Na_V1.7$ peptides were applied acutely to the cells for ~ 10–30 minutes.
For total sodium current (I_{Na}) recordings, the external solution contained (in mM): 130 NaCl, 3 KCl, 30 tetraethylammonium chloride, 1 $CaCl_2$, 0.5 $CdCl_2$, 1 $MgCl_2$, 10 D-glucose and 10 HEPES (pH 7.3 adjusted with NaOH, and mOsm/L= 324). Patch pipettes were filled with an internal solution containing (in mM): 140 CsF, 1.1Cs-EGTA, 10 NaCl, and 15 HEPES (pH 7.3 adjusted with CsOH, and mOsm/L= 311). Peak Na^+ current was acquired by applying 150-millisecond voltage steps from −70 to +60 mV in 5-mV increments from a holding potential of −60 mV to obtain the current-voltage (I-V) relation. Normalization of currents to each cell's capacitance (pF) was performed to allow for collection of current density data. For I-V adjustments, functions were fitted to data using a non-linear least squares analysis (22). I-V curves were fitted using double Boltzmann functions:

$$f = a + g1/(1+\exp((x-V_{1/2}1)/k1)) + g2/(1+\exp(-(x-V_{1/2}2)/k2))$$

where x is the prepulse potential, $V_{1/2}$ is the mid-point potential and k is the corresponding slope factor for single Boltzmann functions. Double Boltzmann fits were used to describe the shape of the curve, not to imply the existence of separate channel populations. Numbers *1* and *2* simply indicate first and second mid-points; *a* along with *g* are fitting parameters.

Activation curves were obtained from the I-V curves by dividing the peak current at each depolarizing step by the driving force according to the equation: $G = I/(V_{mem}-E_{rev})$, where I is the peak current, V_{mem} is the membrane potential and E_{rev} is the reversal potential. The conductance (G) was normalized against the maximum conductance (Gmax). Steady-state inactivation (SSI) curves were obtained by applying an H-infinity protocol that consisted of 1-second conditioning pre-pulses from −120 to +10 mV in 10-mV increments followed by a 200-millisecond test pulse to +10 mV. Inactivation curves were obtained by dividing the peak current recorded at the test pulse by the maximum current (Imax). Activation and SSI curves were fitted with the Boltzmann equation.

In experiments with the Halo-$Na_V1.7$ channels cells were incubated with 200 nM of Halo Ligand Oregon Green for 2 minutes at 37°C. Following this labeling step cells were washed with fresh warm DMEM media 3x to remove unbound ligand. The cells were then left to recover for 30 minutes before recordings

began. In all experiments where this channel was used recordings were performed in the presence of 500 nM TTX in the external solution to block endogenous $Na_V1.7$ currents. During recording small-diameter DRG neurons successfully transfected with the Halo-$Na_V1.7$ plasmid were identified using a fluorescence microscope with stimulation at 490 nm and emission at 520 nm.

In experiments in which clathrin assembly was inhibited, 20 μM of Pitstop2 was added to the cells 30 minutes prior the recordings. When $Na_V1.7$-blocker was employed, ProTx-II was added into the external recording solution at a final concentration of 5 nM.

To isolate potassium currents (I_K), DRG neurons were bathed in external solution composed of (in millimolar): 140 N-methyl-glucamine chloride, 5 KCl, 1 $MgCl_2$, 2 $CaCl_2$, 10 D-glucose and 10 HEPES (pH adjusted to 7.3 with NaOH and mOsm/L= 313). Recording pipettes were filled with internal solution containing (in mM): 140 KCl, 2.5 $MgCl_2$, 4 Mg-ATP, 0.3 Na-GTP, 2.5 $CaCl_2$, 5 EGTA, and 10 HEPES (pH adjusted to 7.3 with KOH and mOsm/L= 320). From a holding potential of -60 mV, I_K activation was determined by applying 300-millisecond voltage steps from −80 to +60 mV in 10-mV increments.

Pipettes were pulled from standard wall borosilicate glass capillaries (Sutter Instruments) with a horizontal puller (Model P-97, Sutter Instruments). The input resistance of the pipettes ranged from 2 to 4 MΩ. Recordings were performed from small DRG neurons with capacitance between 10 and 35 pF (~18-33 μm). Series resistance under 7 MΩ was deemed acceptable. All experiments had a series resistance compensation between 60-90 %. Signals were filtered at 10 kHz and digitized at 10–20 kHz. Analyzes were performed by using Fitmaster software (HEKA) and Origin 9.0 software (OriginLab).

Measurement of action potentials using whole-cell current-clamp electrophysiology. For current-clamp recordings the external solution contained (in millimolar): 154 NaCl, 5.6 KCl, 2 $CaCl_2$, 1 $MgCl_2$, 10 D-Glucose, and 8 HEPES (pH 7.4 adjusted with NaOH, and mOsm/L= 300). The internal solution was composed of (in millimolar): 137 KCl, 10 NaCl, 1 $MgCl_2$, 1 EGTA, and 10 HEPES (pH 7.3 adjusted with KOH, and mOsm/L= 277). At room temperature (22–24°C), whole-cell patch clamp configuration was made, and current-clamp mode was performed to record action potentials. DRG neurons with a resting membrane potential (RMP) more hyperpolarized than −40 mV, stable baseline recordings, and evoked spikes that overshot 0 mV were used for experiments and analysis. The action potentials were evoked by current injection steps from 0–120 pA with an increment of 10 pA in 300 ms. Rheobase was measured by injecting currents from 0 pA with an increment of 10 pA in 50 ms. Analyses were performed by using Fitmaster software (HEKA) and Origin 9.0 software (OriginLab).

Lumbar puncture for intrathecal treatment delivery. Rats between postnatal day 12 and 15 (P12-15) were deeply anesthetized with 4% isoflurane for the induction of anesthesia and 2% for maintenance. The caudal half of the animal's back was shaved and a 25G needle was inserted perpendicular to the spinal column through the L4-L5 intervertebral level and lowered until it met the vertebral body. Occasionally, a quick flicking of the tail could be observed and served as a proxy for optimal needle placement. Entry into the intrathecal space was indicated by a reduction in the pressure necessary to insert the needle. Animals were injected with 10 μL of indicated AAV9 virus containing either AAV-CMV-eGFP-$Na_V1.7$-CRS or AAV-CMV-eGFP-SCR. Electrophysiological recordings were performed two days following the intrathecal injections to allow for cell mediated production of the plasmid encoded peptides.

Preparation of spinal cord for whole-cell patch clamp recordings. Rats were deeply anesthetized with isoflurane (4% for induction and 2% for maintaining). For spinal nerve block, 0.3 mL of 2% lidocaine was injected to both sides of L4 to L5 lumbar vertebrae. Laminectomy was performed from mid-thoracic to low lumbar levels, and the spinal cord was quickly removed to cold modified ACSF oxygenated with 95% O2 and 5% CO2. The ACSF for rat dissection contained the following (in millimolar): 80 NaCl, 2.5 KCl, 1.25 NaH_2PO_4, 0.5 $CaCl_2.2H_2O$, 3.5 $MgCl_2.6H_2O$, 25 $NaHCO_3$, 75 Sucrose, 1.3 ascorbate, 3.0 sodium pyruvate with pH at 7.4 and osmolarity at 310 mOsm. Transverse 400 μm-thick slices were obtained by a vibratome (VT1200S; Leica, Nussloch, Germany). Slices were then incubated for 45 mins at 37°C before a 1h incubation at RT in an oxygenated recording solution containing the following (in millimolar): 125 NaCl, 2.5 KCl, 1.25 $NaH2PO_4$, 2 $CaCl_2.2H_2O$, 1 $MgCl_2.6H2O$, 26 $NaHCO_3$, 25 D-Glucose, 1.3 ascorbate, 3.0 sodium pyruvate with pH at 7.4 and osmolarity at 320 mOsm. The slices were then positioned in a recording

chamber and continuously perfused with oxygenated recording solution at a rate of 3 to 4 mL/min before electrophysiological recordings at room temperature (RT).

Whole-cell patch clamp electrophysiology of spinal cord slices. Second order neurons located in lamina I/IIo of the substantia gelatinosa (SG) were visualized and identified in spinal cord slices using infrared differential interferences contrast video microscopy on an upright microscope (FN1; Nikon, Tokyo, Japan) equipped with a 3.40/0.80 water-immersion objective and near infrared (NIR) charged-coupled device camera (Pco Panda). Micropipettes with resistance of 6 to 10 MΩ when filled with internal solution were fabricated from borosilicate glass (1.5mm OD; Sutter Instruments, Novato, CA) with a four-step micropipette puller (P-97; Sutter Instruments, Novato, CA). The internal solution for recording spontaneous excitatory postsynaptic currents (sEPSC) contained the following (in mM): 120 potassium-gluconate, 20 KCl, 2 $MgCl_2.6H_2O$, 2.0 Na2-ATP, 0.5 Na-GTP, 20 HEPES, 0.5 EGTA with pH at 7.4 and osmolarity at 310 mOsm. In all recordings of spontaneous synaptic activity, whole-cell recording configuration was obtained in voltage-clamp mode and the membrane potential was clamped at -60 mV using a software controlled (PATCHMASTER, HEKA Elektronik, Lambrecht, Germany) digital patch clamp amplifier (EPC10; HEKA Elektronik, Lambrecht, Germany).

The whole-cell configuration was obtained in voltage-clamp mode. To record sEPSCs, bicuculline methiodide (10 μM, Cat# 14343, Sigma Aldrich) and strychnine (2 μM, Cat# S0532, Sigma Aldrich) were added to the recording solution to block γ-aminobutyric acid-activated (GABA) and glycine-activated currents. Hyperpolarizing step pulses (5 mV for 50 milliseconds) were periodically delivered to monitor the access resistance (15-25 MΩ), and recordings were discontinued if the access resistance deviated more than 20% from baseline values. sEPSCs were recorded from each neuron for a total duration of 2 minutes. Currents were sampled at 6 kHz and filtered at 3kHz then analyzed using the Mini-Analysis Program (Synatosoft Inc., NJ) to provide spreadsheets for the generation of cumulative probability plots. The frequency and amplitude of the recordings were compared between neurons from animals in the AAV-SCR and AAV-$Na_V1.7$-CRS treated groups.

AAV plasmid production and encapsulation of pAAV-$Na_V1.7$-CRS in AAV9 capsid. The plasmids pAAV-CMV-eGFP-$Na_V1.7$ and pAAV-CMV-eGFP-SCR were generated by adding the $Na_V1.7$-CRS peptide sequence and the scrambled peptide sequence into the AAV-CMV-eGFP core plasmid (plasmid #67634, Addgene). The sequences were cloned into the plasmid without the terminal lysine in frame following the GFP sequence. The following sequences were inserted into the plasmid: ($Na_V1.7$) – AGCAGGCAGAAGTGCCCACCTTGGTGGTACAGATTCGCCCAC; (SCR) - AAGTACCACCCTTGGGCCTGCTTCAGGCAGTGGAGAAGCCCA. These plasmids were subcloned using the Clone EZ PCR cloning kit with high copy number and resistance to ampicillin (Genscript). Four micrograms of DNA were obtained for each plasmid from Genscript. The plasmids were subsequently packaged into AAV9 viral capsids to test the feasibility of disrupting the interaction between $Na_V1.7$ and CRMP2 as a gene therapy. The encapsulation of the plasmid in AAV serotype 9 capsids was performed by the University of Arizona Viral Core facility. AAV9 particles were produced using HEK293T cells using the triple transfection method and purification of the particles was achieved using an iodixanol centrifugation gradient (23). Cells were transfected when approximately 80-90% confluent and the medium was replaced with previously warmed medium before transfection. The viruses were produced on 10 cm plates and each plate was transfected with 10 of pXR-capsid (pXR-9), 10 μg of recombinant transfer vector, and 10 μg of pHelper vector using polyethyleneimine at a ratio of 4:1. This mixture was incubated briefly at room temperature and then added in single drops to the cell culture medium. After successful transfection, the virus was harvested 72-96h later and isolated using iodixanol density gradient ultracentrifugation (24, 25). The virus was then dialyzed with PBS supplemented with 50 mM NaCl and 0.00001% Pluronic F68 with 50-kDa filters to a final volume near 150 μL.

GPCRome assay. There are ~350 non-olfactory GPCRs, and one third of them are “orphan” since their ligands are unknown. The measurement of G-protein independent β-arrestin recruitment provides a feasible and universal assay platform, since nearly all GPCRs can induce arrestin translocation. Transcriptional activation following arrestin translocation (TANGO) assays are useful for one-target-at-the-time GPCR screening.

PRESTO-TANGO (Parallel Receptor-ome Expression and Screening via Transcriptional Output-TANGO) screens collections of molecules against the druggable human GPCR-ome in a simultaneous fashion. It facilitates the rapid, efficacious, parallel, and simultaneous profiling of biologically active compounds across essentially the entire human druggable GPCR-ome. The TANGO constructs are designed such that upon activation of a GPCR by an agonist, β-arrestin is recruited to the C-terminal sequence of the vasopressin receptor V2. Then, the C-terminal of the GPCR fusion protein is cleaved by TEV protease. The cleavage results in the release of tTA transcription factor which activates the transcription of the luciferase reporter gene [44].

Activation of the D2 GPCR by 100 nM of the D2R agonist quinpirole is used as a positive control. The results are reported as fold change of average basal responses and potential targets are those with responses falling above the >3 fold cutoff. CXCR7 is a frequent hitter in this assay.

Hot plate test. Wild-type female and male mice were placed on a metal plate (Stoelting, Wood Dale, IL) warmed to 52°C and a timer was started. Latency to the first response (flinching or licking the hind paws or jumping) was recorded. A cutoff time of 10 seconds was used to prevent tissue damage, and any mouse that reached the cutoff time was designated the value of the cutoff time as their latency time.

Tail-flick assay. The distal third of the tail of WT female and male mice was immersed in warm water (52°C). Latency to remove the tail from the water (tail-flick latency) was recorded. To prevent tissue damage, a 10-second cutoff was used and animals that did not react before the cutoff were assigned a latency of 10 seconds.

CIPN model of paclitaxel. Paclitaxel was purchased from VCU Health Pharmacy (Athenex, NDC 70860-200-50, Richmond, VA, USA) and dissolved in a 1:1:18 mixture of 200 proof ethanol, kolliphor, and distilled water (Sigma-Aldrich) to a dose of 8 mg/kg. Paclitaxel was then administered intraperitonially every other day for four doses to 8 males and 8 females. The remaining 16 animals received the vehicle 1:1:18 at a volume of 10 ml/kg, i.p. following the same injection regimen. After the final paclitaxel and 1:1:18 injection, these two groups were separated further whereby 4 males and 4 females from each group either received an intrathecal injection of Virus A or Virus B for a total of 4 groups (n = 8/group).

Mechanical and cold sensitivity baselines (time 0) were measured before any injection. Mice were then injected with paclitaxel (8 mg/kg, i.p. every other day for a total of 4 doses) or vehicle and tested at day 7 (mechanical) and 8 (cold) after the first dose of paclitaxel. Mice were then injected intrathecally (µl) and they tested for mechanical (days 14, 16 and 21) and cold (days 15, 17 and 22).

Mechanical sensitivity (von Frey) Test. Mechanical sensitivity thresholds were determined using von Frey filaments as previously described (Chaplan et al., 1994; Bagdas et al., 2015). In brief, the mechanical threshold is expressed as the grams of force required that are required to elicit hind paw withdrawal in 50% of animals.

Cold Sensitivity Test. Mice were individually caged on mesh metal flooring (Bioseb-PVF, Bioseb, Chaville, France) for 30 minutes prior to testing. 20 µL of acetone (Sigma-Aldrich, MO, USA) was applied onto the plantar surface of each hind paw via pipette. The time spent licking, slapping, flinching, or shaking the hind paw was recorded for 60 seconds.

Spared nerve injury (SNI) model of neuropathic pain and intrathecal catheter insertion. The biceps femoris muscle of female and male rats was dissected to expose the 3 terminal branches of the sciatic nerve and perform spared nerve injury by transecting the common peroneal and tibial branches of the right sciatic nerve leaving the sural nerve intact (26). Before any testing, animals were allowed to recover for 5–7 days. Next, rats were sedated using a xylazine/ketamine/ (12/80 mg/kg intraperitoneal; Sigma-Aldrich) and placed in a stereotaxic head holder. Following the exposition and incision of the cisterna magna, an 8-cm catheter (PE-10; Stoelting) was implanted as previously described (27). The von Frey test was performed on the lateral side of the right plantar surface of the rats' hind paws as described by Chaplan et al. (28), before and after 20 µg/5 µl of Myr-TAT-SCR and Myr-TAT-$Na_V1.7$-CRS peptides were intrathecally administered.

Assessment of motor coordination with the Rotarod assay. Following placement of the intrathecal catheters, the rats were trained to walk on a rotating rod (8 rev/min; Rotamex 4/8 device) with a maximal cutoff time of 180 seconds. Training was initiated by placing the rats on a rotating rod and allowing them to walk on the rotating rod until they either fell off or 180 seconds was reached. This process was repeated 6 times and the rats were allowed to recover for 24 hours before beginning the treatment session. Prior to treatment, the rats were run once on a moving rod to establish a baseline value. Treatment, either Myr-TAT-$Na_V1.7$-CRS or Myr-TAT-SCR, was administered spinally via the intrathecal catheter. Assessment consisted of placing the rats on the moving rod and timing until either they fell off or reached a maximum of 180 seconds. This was repeated 30 min after injection and then every hour for a total time course of 5 hours.

Algogram. The analgesic profiles of Myr-TAT-$Na_V1.7$-CRS were analyzed by an in vivo screening tool, ALGOGramTM (ANS Biotech, Riom, France). This platform allowed us to obtain information about the effects of these peptides in 5 different pain areas (Acute and tonic pain, inflammatory pain, neuropathic pain, postoperative pain and visceral pain), by comparing their activity on a battery of 10 validated behavioral pain models with an ANS Biotech reference historical database. Assessment of the efficacy, and analgesic effects of a single administration (4 mg/ml, i.t.) of the peptides to adult male rats were analyzed in the rat models of: Tail flick test in healthy rats, paw pressure test in healthy rats, acetic acid-induced writhing, formalin test, Bennett model of peripheral mononeuropathy, oxaliplatin-induced neuropathy, carrageenan-induced mechanical hyperalgesia, kaolin-induced arthritis, Brennan model of incisional pain; and trinitrobenzene sulfonic acid (TNBS)-induced visceral hypersensitivity.

Statistical methods and data analysis. Graphing and statistical analysis was undertaken with GraphPad Prism (Version 9). All data sets were checked for normality using D'Agostino & Pearson test. Details of statistical tests, significance and sample sizes are reported in the appropriate figure legends. All data plotted represent mean ± SEM. For western blot experiments, statistical differences between groups were determined by Kruskal-Wallis test followed by the Dunn post-hoc test. For electrophysiological recordings: peak current density was compared using Mann-Whitney tests, One-way ANOVA with the Tukey post-hoc test and Kruskal–Wallis test with Dunnett's post-hoc comparisons; $V_{1/2}$ midpoint potential and *k* slope factor, were analyzed with Mann-Whitney test and one-way ANOVA with Tukey post-hoc test; for sensory neuron excitability and action potential waveform parameters, statistical differences between groups were determined using multiple the Mann-Whitney test. Statistical significance of thermal sensitivity was compared by Kruskal-Wallis test followed by the Dunn's post-hoc test. Behavioral data with a time course were analyzed using Multiple Mann-Whitney tests and AUC was analyzed by Mann-Whitney test. For the experiments with paclitaxel analysis of the results did not show any significant differences when animals were separated by sex for any of the outcome measures; thus, males and females were combined. Normality and equality of variances of all data sets except nesting were confirmed by using the Shapiro–Wilk and Levene tests, respectively. All other tests were analyzed with 3-way ANOVA. Post-hoc analysis was performed to determine the source of significant main effects or significant interactions (Holm-Šídák test). For iCGRP release experiments, two-way ANOVA with the Sidak post hoc test was used to determine significance. Motor function differences were analyzed with Multiple Mann-Whitney test.

SI Figures and Legends.

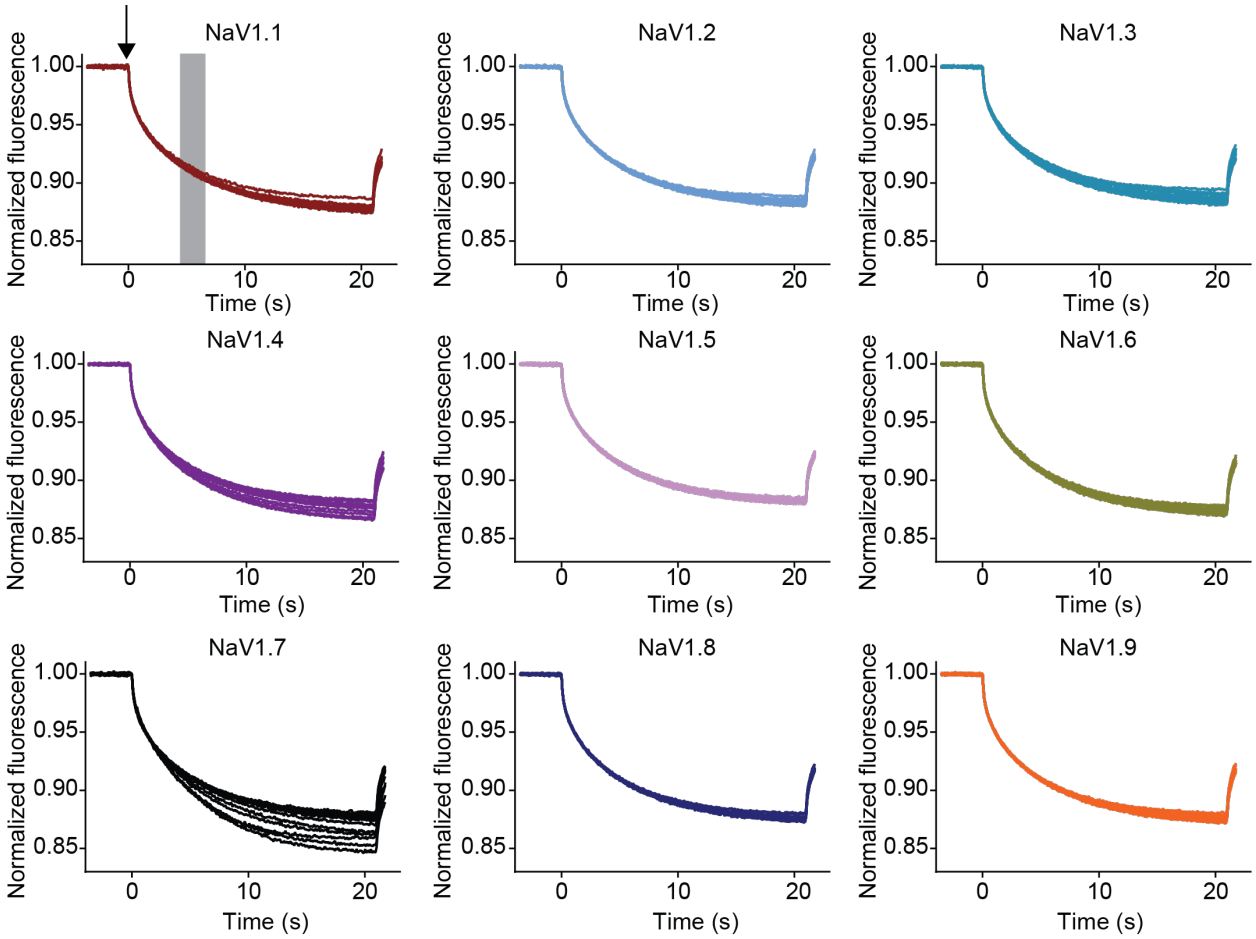

Supplemental figure 1. CRMP2 binding to Na$_V$1.X channel peptides analogous to Na$_V$1.7-CRS. Raw sensorgrams obtained from microscale thermophoresis experiments to determine binding between CRMP2 and peptides derived from intracellular loop 1 of hNa$_V$1.x channels, corresponding to data shown in Figure **1C**. These sensorgrams show the emitted light gathered from capillaries filled with a fluorescently labeled CRMP2 and the corresponding peptide fragment derived from Na$_V$1.7 or the analogous region from all other voltage gated sodium channels. The diffusion of the labeled CRMP2 protein will vary after the application of the thermal stimulus as a function of the binding to the unlabeled test protein included in the capillary. Note that for the Na$_V$1.7 fragment, there is varying degrees of fluorescent emission based on the concentration of the included peptide because this fragment binds to CRMP2. However, there is significantly less spread in the sensorgrams from Na$_V$1.8 and Na$_V$1.9 because these peptide fragments did not bind to CRMP2 and therefore the diffusion was the same across all concentrations. The heating element of the thermophoresis experiment was turned on at the point in time indicated by the arrow. The gray box indicates the region of the curve used for fitting binding parameters.

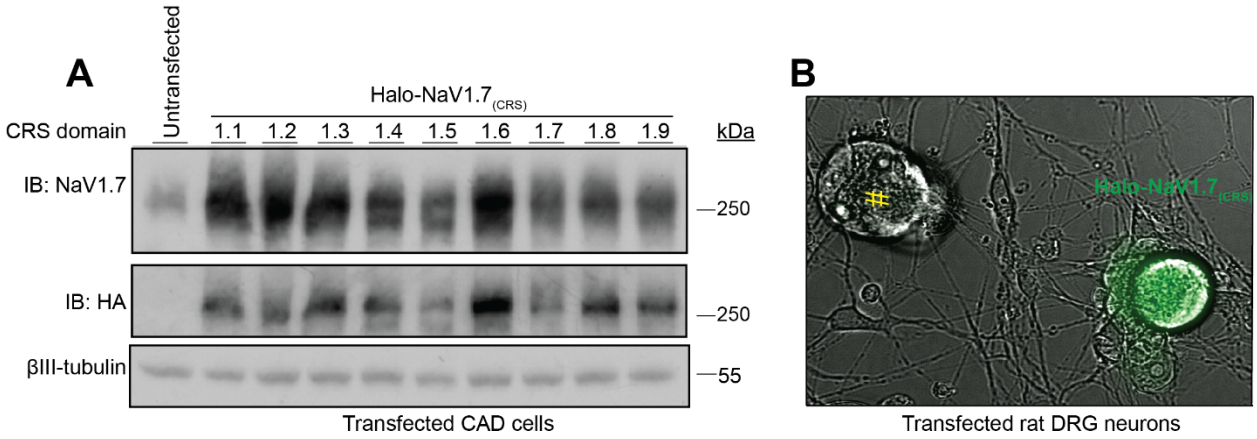

Supplementary figure 2. **Validation of expression for Halo-Na$_V$1.7(1.x) plasmids**. (**A**) Western blots were performed after transfecting each Halo-Na$_V$1.7(1.x) plasmid into CAD cells to verify the expression of channels in a cellular context. Each channel was constructed with an HA tag immediately adjacent to the HaloTag sequence, which allowed for identification of the overexpressed constructs separately from the endogenously expressed channels found in CAD cells. (**B**) DRGs from female rats transfected with the Halo-Na$_V$1.7$_{(WT)}$ channel and labeled with Oregon Green Halo Ligand. Note the non-transfected neuron labeled with the yellow hash sign.

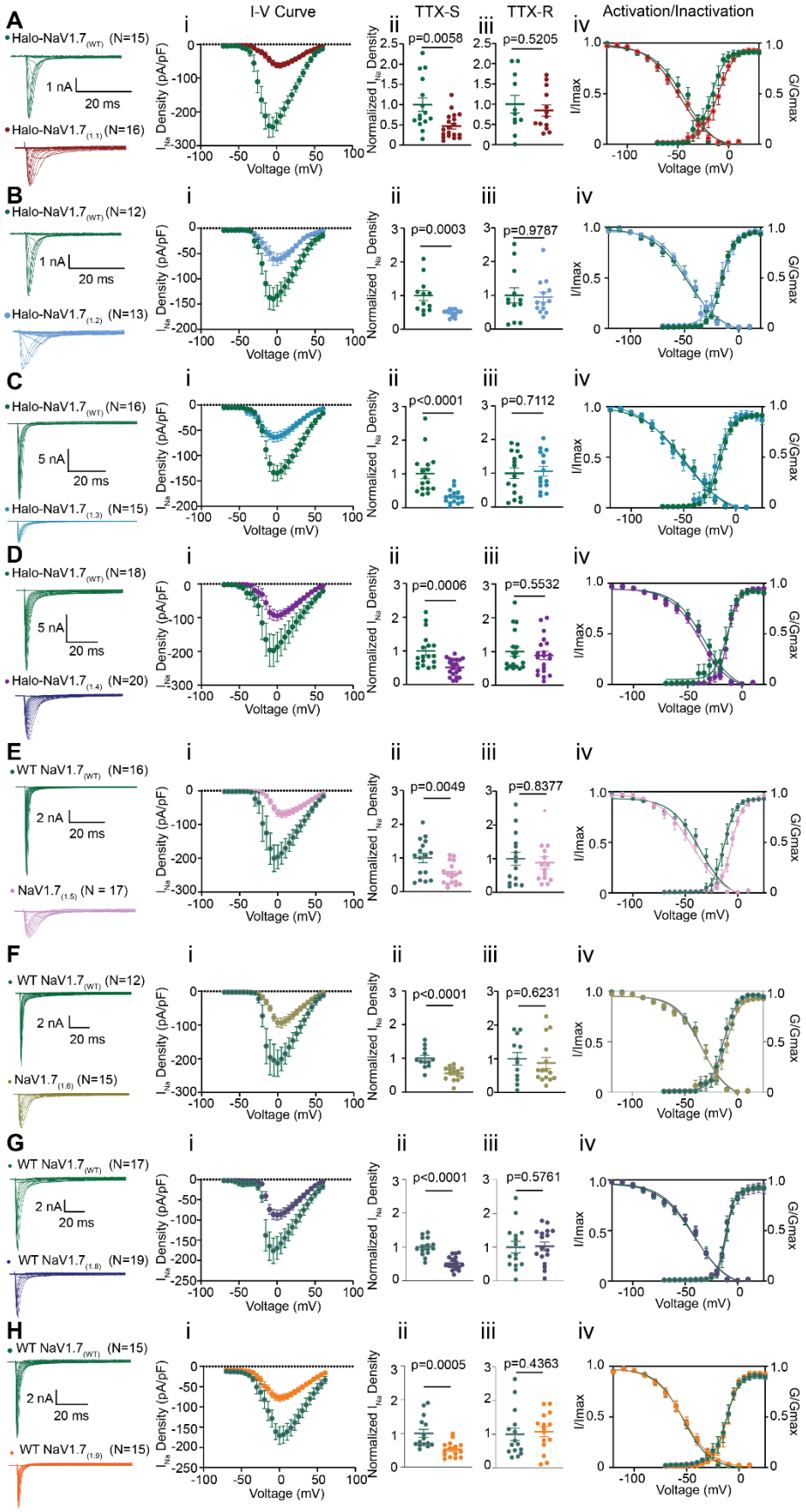
A
Halo-NaV1.7(WT) (N=15)
1 nA
20 ms
Halo-NaV1.7(1.1) (N=16)
I-V Curve
TTX-S
TTX-R
Activation/Inactivation
i
ii
iii
iv
p=0.0058
p=0.5205
Density (pA/pF)
Normalized INa Density
I/Imax
G/Gmax
Voltage (mV)
B
Halo-NaV1.7(WT) (N=12)
1 nA
20 ms
Halo-NaV1.7(1.2) (N=13)
p=0.0003
p=0.9787
C
Halo-NaV1.7(WT) (N=16)
5 nA
20 ms
Halo-NaV1.7(1.3) (N=15)
p<0.0001
p=0.7112
D
Halo-NaV1.7(WT) (N=18)
5 nA
20 ms
Halo-NaV1.7(1.4) (N=20)
p=0.0006
p=0.5532
E
WT NaV1.7(WT) (N=16)
2 nA
20 ms
NaV1.7(1.5) (N = 17)
p=0.0049
p=0.8377
F
WT NaV1.7(WT) (N=12)
2 nA
20 ms
NaV1.7(1.6) (N=15)
p<0.0001
p=0.6231
G
WT NaV1.7(WT) (N=17)
2 nA
20 ms
WT NaV1.7(1.8) (N=19)
p<0.0001
p=0.5761
H
WT NaV1.7(WT) (N=15)
2 nA
20 ms
WT NaV1.7(1.9) (N=15)
p=0.0005
p=0.4363

1

Supplementary figure 3. Swapping the Na$_V$1.7-CRMP2 regulatory segment with the analogous domain from NaV1.1-NaV1.9 channels reduces TTX-S currents but spares TTX-R currents. Representative traces of sodium currents recorded from rat DRG sensory neurons transfected with Halo-Na$_V$1.7$_{(WT)}$ and (**A**) Halo-Na$_V$1.7$_{(1.1}$), (**B**) Halo-Na$_V$1.7$_{(1.2)}$, (**C**) Halo-Na$_V$1.7$_{(1.3)}$, (**D**) Halo-Na$_V$1.7$_{(1.4)}$, (**E**) Halo-Na$_V$1.7$_{(1.5}$), (**F**) Halo-Na$_V$1.7$_{(1.6)}$, (**G**) Halo-Na$_V$1.7$_{(1.8)}$, and (**H**) Halo-Na$_V$1.7$_{(1.9}$). (*i*) Current density-voltage relationship for the indicated Halo-Na$_V$1.7 channels. (*ii*) TTX-S peak current density for the indicated Halo-Na$_V$1.7$_{(1.x)}$ channel compared to its own Halo-Na$_V$1.7$_{(WT)}$ control. (*iii*) TTX-R peak current density for the indicated Halo-Na$_V$1.7$_{(1.x)}$ channel compared Halo-Na$_V$1.7$_{(WT)}$, (*iv*) Biophysical properties of voltage-dependent activation and steady-state inactivation of the previously indicated channels. Values for $V_{1/2}$ and slope (*k*) can be found in Table S1; N=12-20 cells; error bars indicate mean ± SEM; *p* values as indicated; Mann-Whitney test.

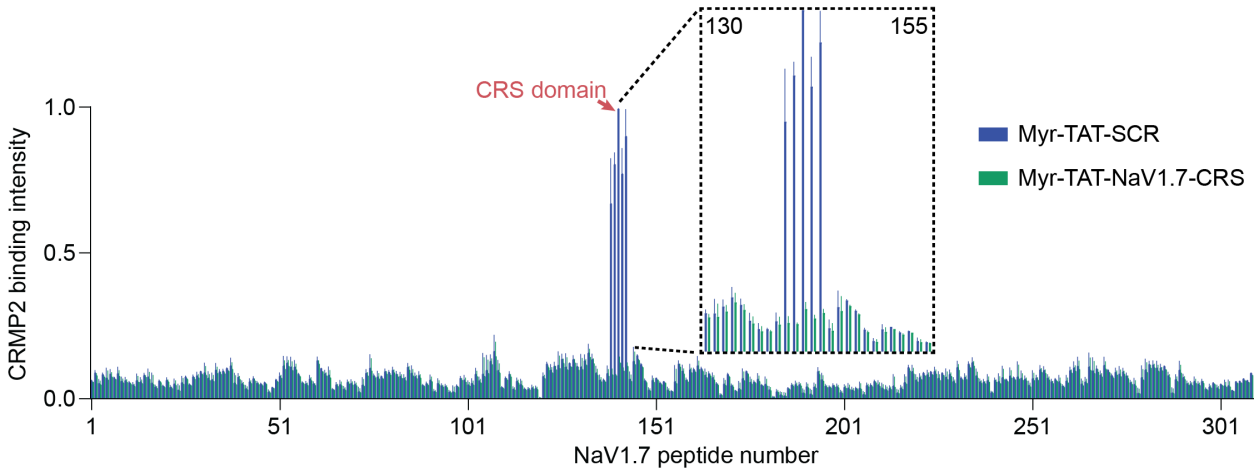

Supplementary figure 4. Treatment with Myr-TAT-Na$_V$1.7-CRS reduces CRMP2 binding to the CRS domain in rat spinal cord lysate. Spinal cord lysates from rats were incubated with Myr-TAT-Na$_V$1.7-CRS or Myr-TAT-SCR and binding to the peptide microarray was assessed. Treatment with Myr-TAT-Na$_V$1.7-CRS (5 μM) significantly reduced the binding between CRMP2 and the CRS domain on the microarray.

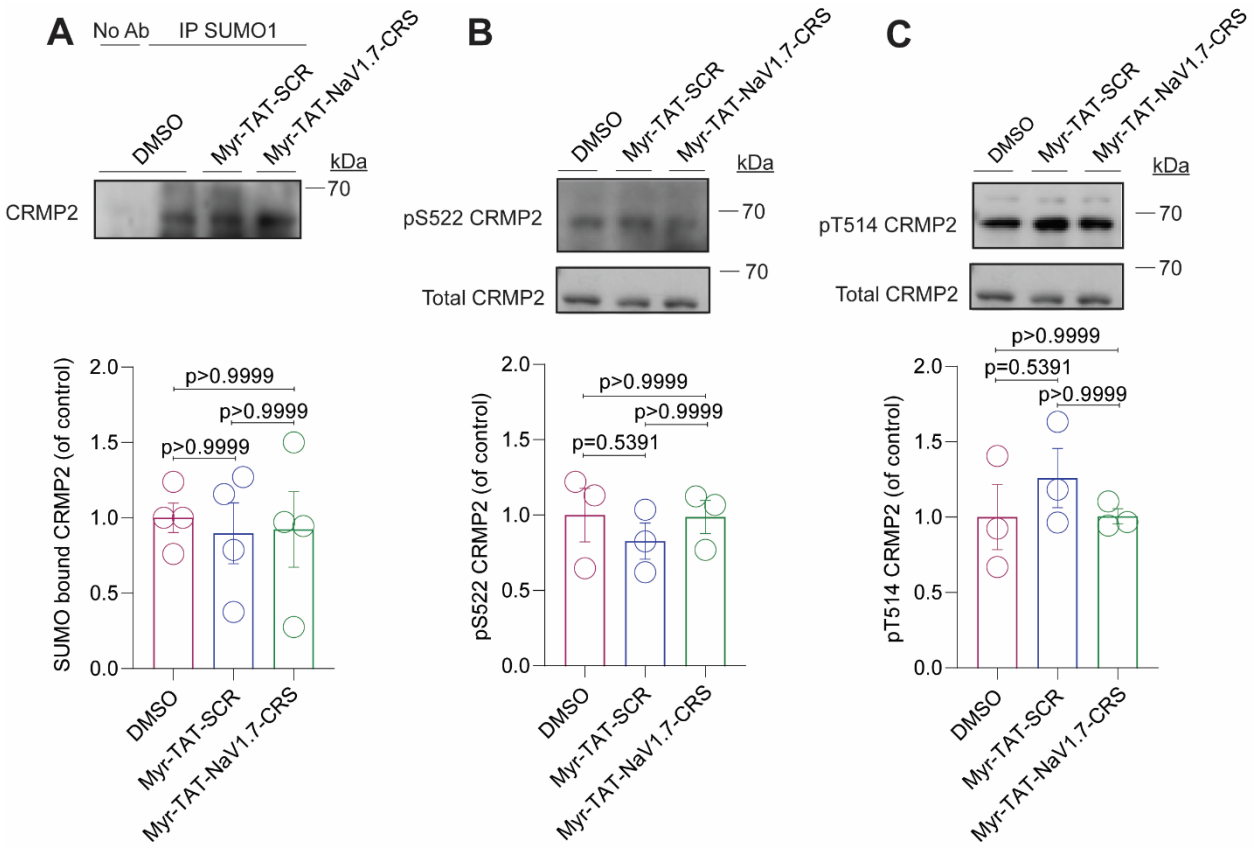

Supplementary figure 5. Myr-TAT-Nav1.7-CRS does not affect CRMP2 SUMOylation or phosphorylation. (**A**) Representative immunoblot (Top) and summary (Bottom) to detect SUMOylated CRMP2 from CAD cells treated with indicated peptides (n=4). (**B, C**) Representative immunoblots of CAD cells lysates indicating CRMP2 phosphorylation levels at indicated kinase target sites (n=3; Top), and quantitative analysis of CRMP2 phosphorylation compared with total CRMP2 (Bottom). Error bars show mean ± SEM; *p* values as indicated; Kruskal-Wallis test followed by the Dunn post hoc test.

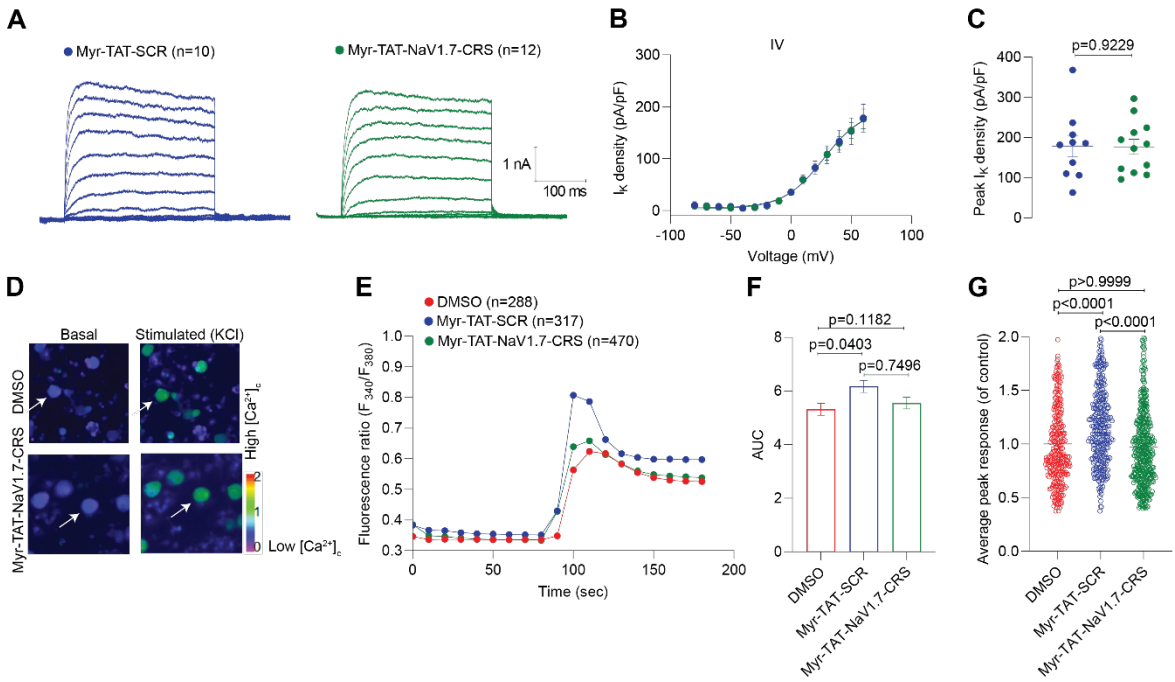

Supplementary figure 6. Myr-TAT-Na$_V$1.7-CRS peptide does not affect voltage-gated potassium and calcium channels. (**A**) Representative potassium current traces recorded from sensory neurons in the presence of 5 μM of Myr-TAT-SCR and Myr-TAT-Na$_V$1.7-CRS peptides. (**B**) Double Boltzmann fits for current density-voltage curves. (C) Summary of peak current densities (pA/pF). N=10-12 cells; error bars indicate mean ± SEM; *p* values as indicated; Mann-Whitney test. (**D**) Pseudo colored fluorescent images of a field of DRG neurons visualized for Fura-2AM, before (Basal) and after stimulation with 90 mM KCl for control (0.05% of DMSO) and 5 μM Myr-TAT-Na$_V$1.7-CRS peptides treated neurons. Following a 1-min baseline measurement, neurons were stimulated with 90 mM KCl for 10 s. Exemplar images of the neurons (white arrows) at basal and peak calcium are indicated. (**E**) The average change in fluorescence ratio (F_{340}/F_{380}) over time for vehicle-treated (red circles), Myr-TAT-SCR treated (blue circles) or Myr-TAT-Na$_V$1.7-CRS treated (green circles) neurons; all error bars are smaller than the symbols. Summary graph of the average area under the curve (AUC) between 80 and 180 s (**F**) and the peak fluorescence response (adjusted for background) (**G**) of rat neurons treated as indicated. N=288-470 cells; error bars indicate mean ± SEM; *p* values as indicated; One-way ANOVA with the Tukey's post-hoc test (**F**) and Kruskal-Wallis test with the Dunn's post hoc test (**G**).

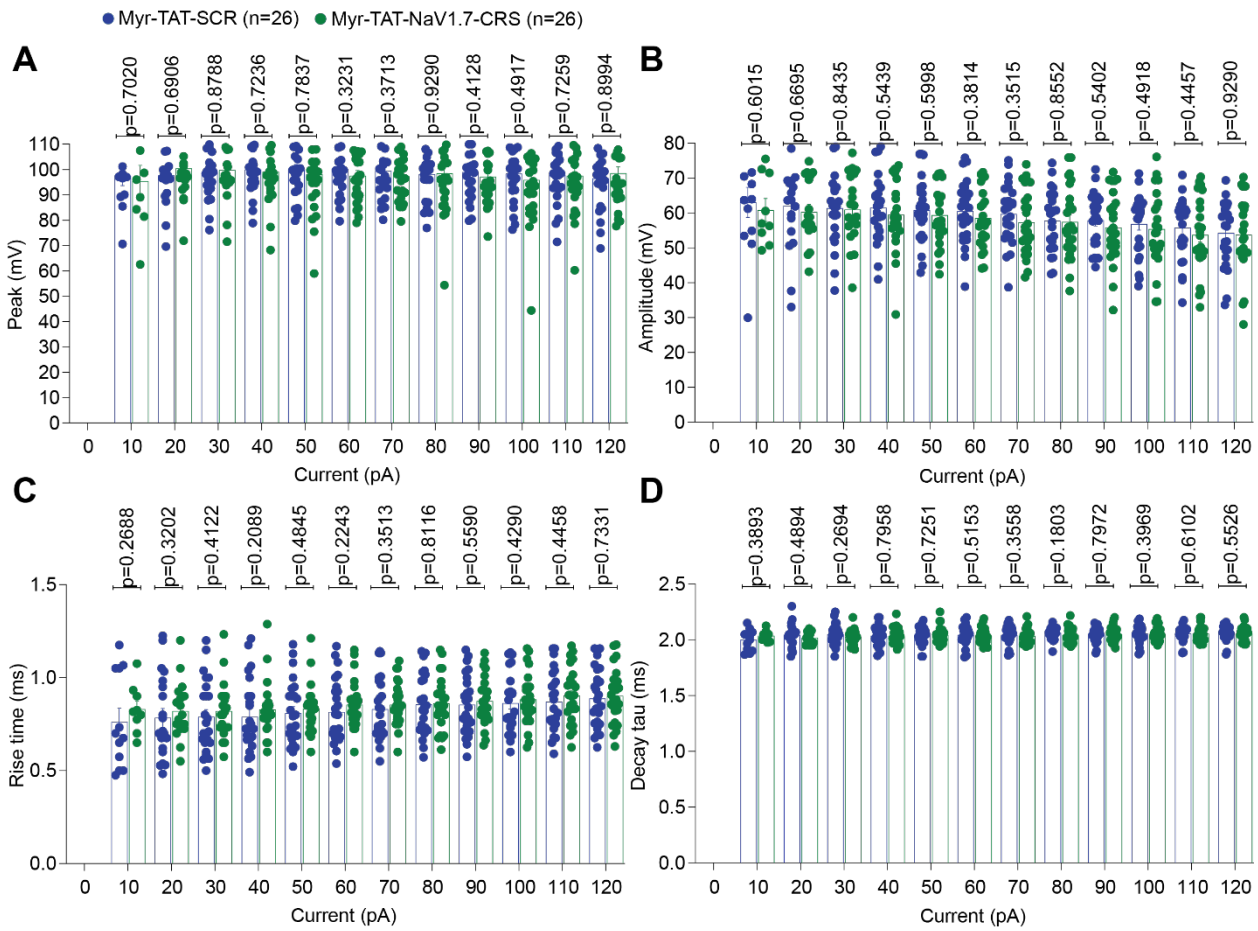

Supplementary figure 7. Sensory neuron AP waveform parameters are not affected by acute treatment with the Myr-TAT-NaV1.7-CRS peptide. Summary of the action potential peak (in mV) (**A**), amplitude (in mV) (**B**), rise time (in ms) (**C**), and decay time (in ms) (**D**), after incubation with 5 μM of Myr-TAT-SCR or Myr-TAT-Nav1.7-CRS peptides. N=26 cells; error bars indicate mean ± SEM; *p* values as indicated; Multiple Mann-Whitney test.

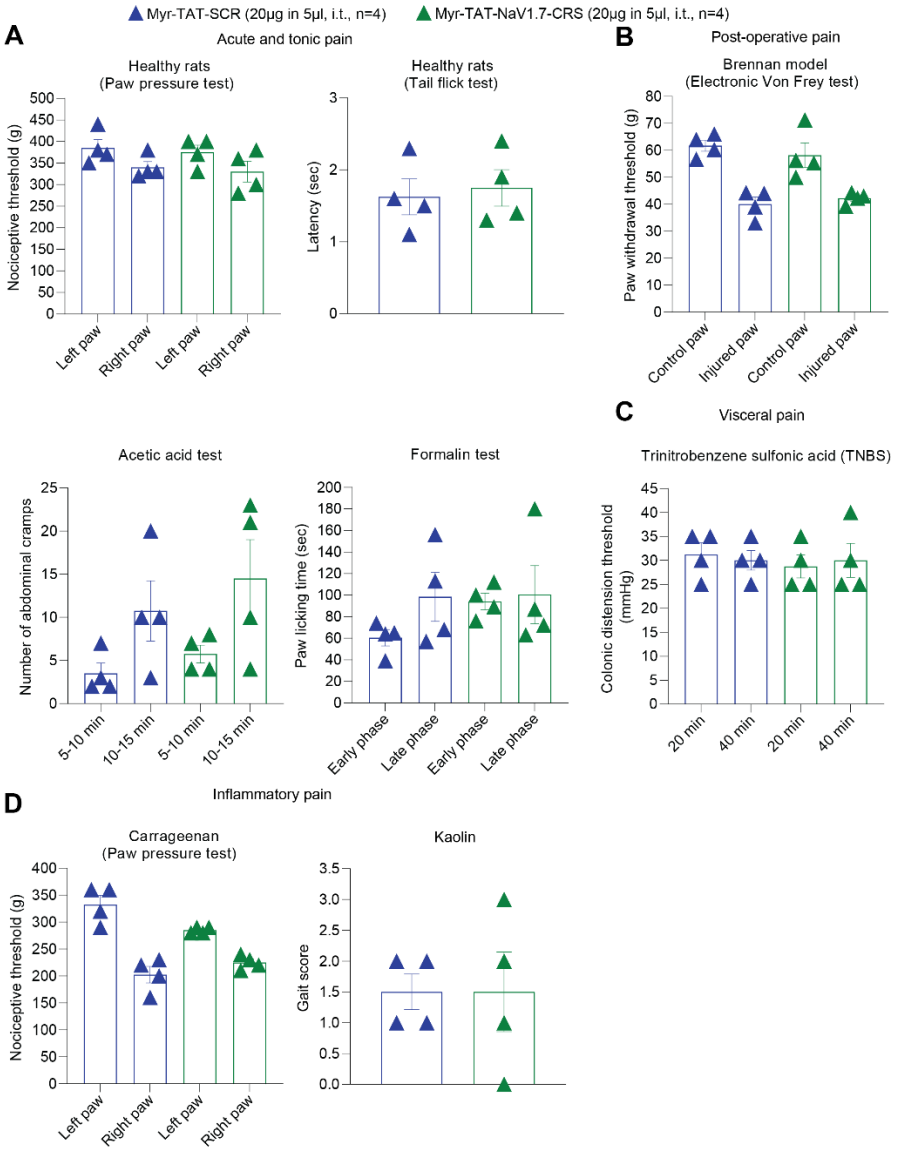

Supplementary figure 8. Disruption of coupling between CRMP2 and Nav1.7 does not influence outcomes of acute pain assays. All behavioral assays were performed in male rats following a single 20 µg in 5 µl i.t. dose of either Myr-TAT-SCR (blue, n=4) or Myr-TAT-Nav1.7-CRS (green, n=4). (**A**) Top: Paw pressure test and the tail flick test demonstrated no effect on acute and tonic pain in healthy rats. Bottom: The number of abdominal cramps recorded for each group was not different between treatment categories for the acetic acid test. In the formalin test there were no differences observed between treatment groups in either the early or late phase as measured by paw licking time. (**B**) The Brennan model of post-surgical pain and (**C**) the model of trinitrobenzene sulfonic acid (TNBS) induced visceral pain. (**D**) Carrageenan and Kaolin were applied to the plantar surface of the paw and nociceptive thresholds and a gate score were determined. No effect was observed between groups treated with either peptide. Error bars indicated ± SEM; p values as indicated; Significant differences were determined using a Mann-Whitney test.

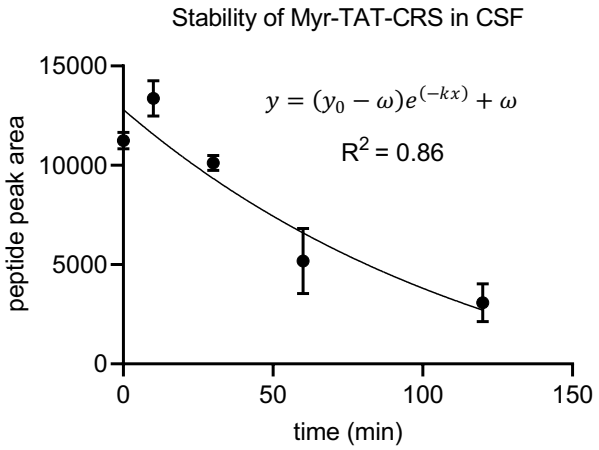

Supplementary figure 9. Determination of the stability of Myr-TAT-Nav1.7-CRS peptide. The % remaining of Myr-TAT-Nav1.7-CRS peptide after incubation in rat plasma was calculated using the following equation: % Remaining = 100 x (PAR at appointed incubation time / PAR at T0 time), where PAR is the peak area ratio of analyte versus internal standard (IS). The appointed incubation time points were T0 (0 min), Tn (n=0,10,30,60,120 min). The half-life (t1/2) was calculated from a plot of peak area over time fit with a one phase exponential decay function. The peak area from the LC/MS/MS raw data was fit with a one phase exponential decay function of the form outlined below:

$$y = (y_0 - \omega)e^{(-kx)} + \omega$$

Where:

$$y_0 = 12{,}806 = quantity\ at\ t_0$$

$$\omega = -3{,}795 = plateau$$

$$k = 0.0007805 = \ rate\ constant$$

From this fit we were able to determine the rate constant for the decay of the peptide in CSF (k), which equals 0.0007805. Then, assuming first order decay kinetics we can calculate the half-life using the following equation:

$$t_{1/2} = \frac{ln2}{k}$$

Solving this equation for k=0.0007805 yields a half-life of ~88 minutes.

It is well established that the in vivo half-life of a peptide is typically much shorter than the stability measured in vitro using serum or CSF. This can be explained by the dynamic nature of biological systems, including factors such as enzymatic degradation, renal excretion, and other clearance mechanisms, which all contribute to the accelerated elimination of the peptide within a living organism. We recognize that while the half-life of the Myr-TAT-Nav1.7-CRS peptide in CSF is sufficiently long to explain the analgesic effect we observed, it is possible that the peptide is degraded more quickly in vivo. This would then suggest that the analgesic effect of the peptide lasts longer than the half-life of the peptide in the intact system.

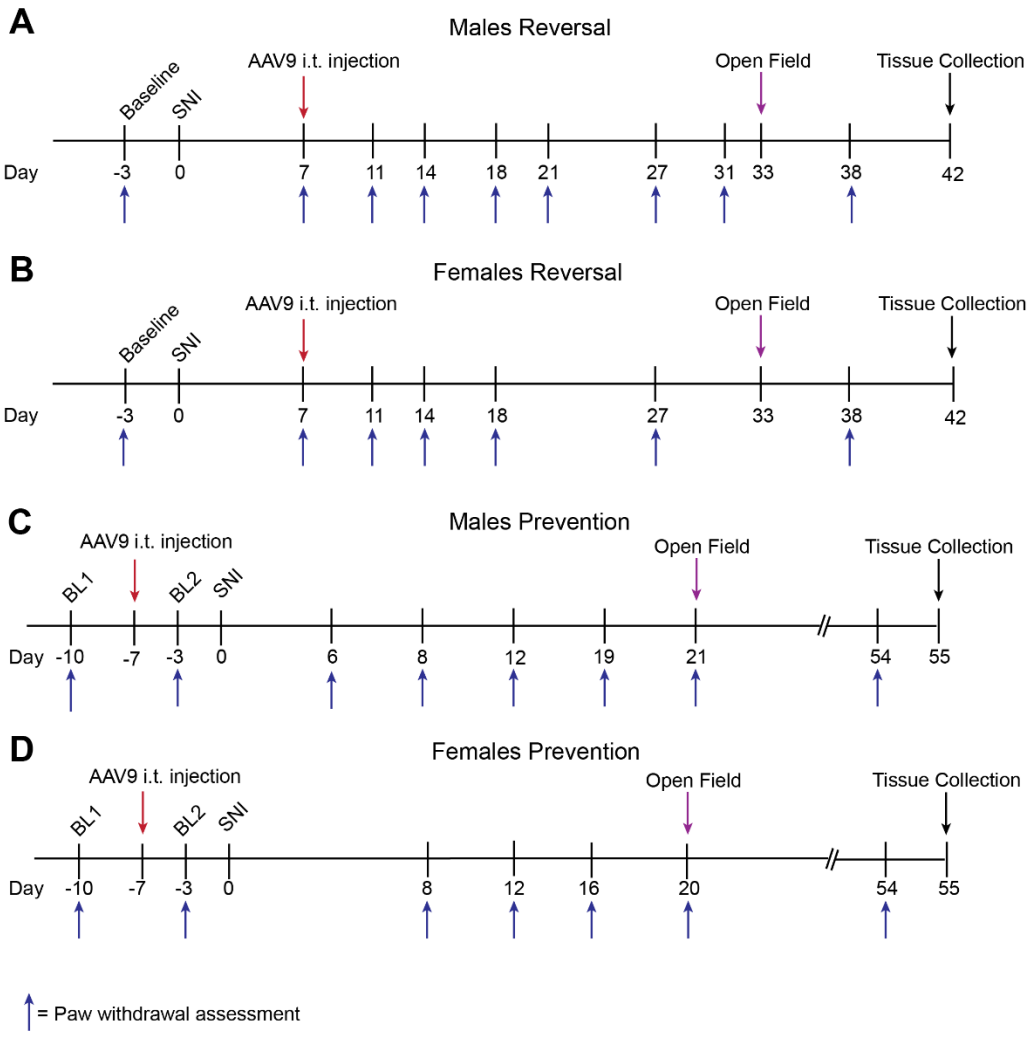

Supplementary figure 10. Experimental timelines of paw withdrawal assessment, locomotor activity and anxiety-like behaviors from male and female mice with SNI. (**A**) Male reversal timeline indicating assessment of mechanical allodynia at days -3, 7, 11, 14, 18, 21, 27, 31, and 38. AAV9 was intrathecally injected 7 days after SNI. Open field test was performed at day 33 and tissue was collected at day 42 after SNI. (**B**) Female reversal timeline indicating assessment of mechanical allodynia at days -3, 7, 11, 14, 18, 27, and 38. AAV9 was intrathecally injected 7 days after SNI. Open field test was performed at day 33 and tissue was collected 42 days after SNI. (**C**) Male prevention timeline indicating assessment of paw withdrawal at days -10, -3, 6, 8, 12, 19, 21, and 54. AAV9 was injected 7 days before SNI. Open field test was performed at day 21 and tissue was collected at day 55 after SNI. (**D**) Female prevention timeline indicating assessment of paw withdrawal at days -10, -3, 8, 12, 16, 20, and 54. AAV9 was injected 7 days before SNI. Open field test was performed at day 20 after SNI and tissue collection at day 55 after SNI.

SI Tables

Table S1. Biophysical properties of Halo-Na$_V$1.7(WT) channels and Halo-Na$_V$1.7(X.X) mutants.

	Halo-Na$_V$1.7(WT)	*Halo-Na$_V$1.7(1.1)*
Activation		
$V_{1/2}$	-17.496 ± 1.198 (15)	-10.538 ± 1.063 (16)
k	7.471 ± 1.077 (15)	8.204 ± 0.960 (16)
Inactivation		
$V_{1/2}$	-43.182 ± 2.203 (15)	-48.369 ± 1.667 (16)
k	-15.851 ± 2.138 (15)	-15.692 ± 1.662 (16)
	Halo-Na$_V$1.7(WT)	*Halo-Na$_V$1.7(1.2)*
Activation		
$V_{1/2}$	-15.811 ± 0.638 (12)	-15.811 ± 1.277 (13)
k	5.295 ± 0.446 (12)	7.748 ± 1.156 (13)
Inactivation		
$V_{1/2}$	-47.307 ± 2.044 (12)	-45.667 ± 1.737 (13)
k	-15.826 ± 2.035 (12)	-15.612 ± 1.645 (13)
	Halo-Na$_V$1.7(WT)	*Halo-Na$_V$1.7(1.3)*
Activation		
$V_{1/2}$	-15.196 ± 0.765 (15)	-17.324 ± 1.183 (16)
k	6.165 ± 0.792 (15)	6.491 ± 1.051 (16)
Inactivation		
$V_{1/2}$	-47.590 ± 3.319 (15)	-51.706 ± 3.260 (16)
k	-20.832± 3.698 (15)	-21.118 ± 3.776 (16)
	Halo-Na$_V$1.7(WT)	*Halo-Na$_V$1.7(1.4)*
Activation		
$V_{1/2}$	-14.888 ± 1.221 (18)	-12.678 ± 0.561(20)
k	5.888 ± 1.076 (18)	4.161 ± 0.488 (20)
Inactivation		
$V_{1/2}$	-40.564 ± 1.410 (18)	-42.828 ± 1.432 (20)
k	-13.607 ± 1.304 (18)	-14.3.73 ± 1.355 (20)
	Halo-Na$_V$1.7(WT)	*Halo-Na$_V$1.7(1.5)*
Activation		
$V_{1/2}$	-13.023 ± 0.791 (15)	-5.748 ± 0.507 (14)
k	5.504 ± 0.694(15)	5.282 ± 0.440 (14)
Inactivation		
$V_{1/2}$	-43.750 ± 1.313(15)	-43.053 ± 1.473 (14)
k	-16.615 ± 1.296 (15)	-15.696 ± 1.424 (14)
	Halo-Na$_V$1.7(WT)	*Halo-Na$_V$1.7(1.6)*
Activation		
$V_{1/2}$	-13.297 ± 0.916 (12)	-10.434 ± 0.862 (15)
k	6.087 ± 0.808 (12)	6.413 ± 0.759 (15)
Inactivation		
$V_{1/2}$	-33.958 ± 1.537 (12)	-34.189 ± 1.419 (15)
k	-12.141 ± 1.351 (12)	-13.077 ± 1.250 (15)

	Halo-Na$_V$1.7(WT)	*Halo-Na$_V$1.7(1.8)*
Activation		
$V_{1/2}$	-10.540 ± 0.539 (15)	-11.535 ± 0.557 (17)
k	3.992 ± 0.468 (15)	4.189 ± 0.484 (17)
Inactivation		
$V_{1/2}$	-41.582 ± 1.901 (15)	-41.428 ± 1.612 (17)
k	-16.574 ± 1.838 (15)	-15.696 ± 1.538 (17)
	Halo-Na$_V$1.7(WT)	*Halo-Na$_V$1.7(1.9)*
Activation		
$V_{1/2}$	-12.167 ± 0.852 (15)	-11.754 ± 0.743 (15)
k	6.128 ± 0.750 (15)	5.496 ± 0.651 (15)
Inactivation		
$V_{1/2}$	-53.446 ± 1.114 (15)	-53.160 ± 1.524 (15)
k	-12.789 ± 1.053 (15)	-13.964 ± 1.477 (15)

Values are means ± SEM calculated from fits of the data from the indicated number of individual cells (in parentheses) to the Boltzmann equation; $V_{1/2}$ midpoint potential (mV) for voltage-dependent of activation or inactivation; *k*, slope factor. These values pertain to Fig. S3. Data were analyzed with Mann-Whitney test. Details of statistical comparisons are shown in Table S5.

Table S2. Sodium channel gating properties following treatment with Myr-TAT-Na$_V$1.7-CRS or Myr-TAT-SCR control peptide.

	Myr-TAT-SCR		*Myr-TAT*-Na$_V$1.7-*CRS*	
Activation				
$V_{1/2}$	-20.891 ± 0.491 (10)		-18.222 ± 1.057 (9)	
k	3.451 ± 0.427 (10)		6.619 ± 0.945 (9)	
Inactivation				
$V_{1/2}$	-49.661 ± 1.074 (14)		-48.744 ± 2.074 (13)	
k	-11.625 ± 1.063 (14)		-15.436 ± 2.330 (13)	
	Myr-TAT-SCR + Vehicle	*Myr-TAT-SCR + 5 nM ProTx-II*	*Myr-TAT*-Na$_V$1.7-*CRS + Vehicle*	*Myr-TAT*-Na$_V$1.7-*CRS + 5 nM ProTx-II*
Activation				
$V_{1/2}$	-21.796 ± 0.886 (12)	-11.790 ± 1.451 (11)	-16.754 ± 0.688 (11)	-13.379 ± 1.549 (7)
k	6.478 ± 0.792 (12)	9.025 ± 1.292 (11)	5.930 ± 0.608 (11)	8.568 ± 1.398 (7)
Inactivation				
$V_{1/2}$	-55.752 ± 1.149 (11)	-56.185 ± 2.578 (11)	-61.788 ± 1.600 (10)	-65.578 ± 1.562 (6)
k	-10.245 ± 1.084 (11)	-13.761 ± 2.662 (11)	-10.594 ± 1.474 (10)	-10.875 ± 1.389 (6)
	Myr-TAT-SCR + siRNA-Control	*Myr-TAT-SCR + siRNA-CRMP2*	*Myr-TAT*-Na$_V$1.7-*CRS + siRNA-Control*	*Myr-TAT*-Na$_V$1.7-*CRS + siRNA-CRMP2*
Activation				
$V_{1/2}$	-18.817 ± 1.031(8)	-16.842 ± 1.082 (10)	-14.997 ± 0.707(10)	-18.547 ± 1.0 (10)
k	7.885 ± 0.945 (8)	7.682 ± 0.983 (10)	6.970 ± 0.632 (10)	7.644 ± 0.912 (10)
Inactivation				
$V_{1/2}$	-58.378 ± 1.822 (10)	-64.102 ± 1.470 (7)	-62.284 ± 1.388 (10)	-62.143 ± 1.903 (11)
k	-13.012 ± 1.740 (10)	-11.331 ± 1.336 (7)	-11.090 ± 1.267 (10)	-13.542 ± 1.797(11)
	Myr-TAT-SCR + DMSO	*Myr-TAT-SCR + 20 µM Pitstop2*	*Myr-TAT*-Na$_V$1.7-*CRS + DMSO*	*Myr-TAT*-Na$_V$1.7-*CRS + 20 µM Pitstop2*
Activation				
$V_{1/2}$	-18.909 ± 0.689 (14)	-14.236 ± 0.904 (7)	-17.872 ± 1.466 (11)	-18.871 ± 0.998 (13)
k	4.940 ± 0.603 (14)	6.915 ± 0.805 (7)	8.347 ± 1.355 (11)	7.629 ± 0.911 (13)
Inactivation				
$V_{1/2}$	-54.698 ± 1.188 (9)	-61.458 ± 1.217 (7)	-61.391 ± 0.780 (8)	-61.199 ± 0.997 (10)
k	-11.740 ± 1.116 (9)	-7.550 ± 1.072 (7)	-10.437 ± 0.707 (8)	-9.674 ± 0.897 (10)

Values are means ± SEM calculated from fits of the data from the indicated number of individual cells (in parentheses) to the Boltzmann equation; $V_{1/2}$ midpoint potential (mV) for voltage-dependent of activation or inactivation; k, slope factor. These values pertain to Figure 2. See supplementary statistical table for details of all statistical tests comparing differences between groups. Data were analyzed with Mann-Whitney test and one-way ANOVA with Tukey post hoc test; All statistical tests are shown in Table S5. DMSO, dimethylsulfoxide; ANOVA, analysis of variance.

Table S3. Biophysical properties of sodium currents following genetic delivery of interfering peptide in rat DRG neurons.

	AAV-SCR		*AAV-Na$_V$1.7-CRS*	
Activation				
$V_{1/2}$	-17.370 ± 0.491 (12)		-17.945 ± 1.057 (12)	
k	8.232 ± 0.427 (12)		8.028 ± 0.945 (12)	
Inactivation				
$V_{1/2}$	-50.230± 1.074 (12)		-49.320 ± 2.074 (12)	
k	-11.890 ± 1.063 (12)		-13.061 ± 2.330 (12)	
	AAV-SCR + Vehicle	*AAV-SCR + 5 nM ProTx-II*	*AAV-Na$_V$1.7-CRS + Vehicle*	*AAV-Na$_V$1.7-CRS + 5 nM ProTx-II*
Activation				
$V_{1/2}$	-24.449 ± 0.620 (15)	-12.156 ± 0.922 (12)	-26.747 ± 0.858 (13)	-24.001 ± 1.311 (15)
k	5.797 ± 0.546 (15)	7.247 ± 0.823 (12)	5.349 ± 0.752 (13)	8.170 ± 1.207 (15)
Inactivation				
$V_{1/2}$	-52.147 ± 1.614 (15)	-44.326 ± 2.692 (12)	-58.741 ± 1.605 (13)	-52.516 ± 2.214 15)
k	-18.065 ± 1.728 (15)	-18.956 ± 2.78 (12)	-15.255 ± 1.598 (13)	-18.334 ± 2.389 (15)
	AAV-SCR + DMSO	*AAV-SCR + 20 µM Pitstop2*	*AAV-Na$_V$1.7-CRS + DMSO*	*AAV-Na$_V$1.7-CRS + 20 µM Pitstop2*
Activation				
$V_{1/2}$	-21.946 ± 1.720 (12)	-25.782 ± 1.874 (15)	-23.054 ± 1.262 (15)	-17.621 ± 2.441 (9)
k	8.521 ± 1.598 (12)	9.756 ± 1.797 (15)	8.063 ± 1.159 (15)	11.247 ± 2.432 (9)
Inactivation				
$V_{1/2}$	-49.001 ± 1.848 (12)	-47.284 ± 1.497 (15)	-55.146 ± 1.664 (15)	-48.747 ± 1.592 (9)
k	-15.754 ± 1.850 (12)	-14.758 ± 1.457 (15)	-14.475 ± 1.634 (15)	-13.477 ± 1.518 (9)

Values are means ± SEM calculated from fits of the data from the indicated number of individual cells (in parentheses) to the Boltzmann equation; $V_{1/2}$ midpoint potential (mV) for voltage-dependent of activation or inactivation; *k*, slope factor. These values pertain to biophysical properties of recordings from Fig. 7. See supplemental statistical table for details of all statistical comparisons between groups. Data were analyzed with Mann-Whitney test and one-way ANOVA with Tukey post hoc test. All statistical tests are shown in Table S5. DRG, dorsal root ganglia; DMSO, dimethylsulfoxide; ANOVA, analysis of variance.

Table S4. Biophysical properties of sodium currents following genetic delivery of interfering peptide in macaque DRG neurons.

	AAV9-SCR + TTX		*AAV9-Na_V1.7-CRS+ TTX*	
Activation				
$V_{1/2}$	-7.361 ± 1.232 (11)		-8.037 ± 1.238 (11)	
k	4.992 ± 1.072 (11)		4.151 ± 1.074 (11)	
	AAV9-SCR + Vehicle	*AAV9-SCR + 5 nM ProTx-II*	*AAV9-Na_V1.7-CRS+ Vehicle*	*AAV9-Na_V1.7-CRS+ 5 nM ProTx-II*
Activation				
$V_{1/2}$	-26.624 ± 1.017 (13)	-19.767 ± 1.500 (13)	-25.920 ± 0.890 (17)	-23.060 ± 1.480 (14)
k	4.824 ± 0.892 (13)	6.424 ± 1.339 (13)	3.177 ± 0.771 (17)	6.320 ± 1.327 (14)

Values are means ± SEM calculated from fits of the data from the indicated number of individual cells (in parentheses) to the Boltzmann equation; $V_{1/2}$ midpoint potential (mV) for voltage-dependent of activation or inactivation; *k*, slope factor. These values pertain to biophysical properties of recordings from Fig. 7. See supplemental statistical table for details of all statistical comparisons. Data were analyzed with Mann-Whitney test and one-way ANOVA with Tukey's post hoc test. All statistical tests are shown in Table S5. DRG, dorsal root ganglia; DMSO, dimethylsulfoxide; ANOVA, analysis of variance.

SI References

1. J. M. Brittain *et al.*, Suppression of inflammatory and neuropathic pain by uncoupling CRMP-2 from the presynaptic Ca(2)(+) channel complex. *Nat Med* **17**, 822-829 (2011).
2. L. François-Moutal *et al.*, A membrane-delimited N-myristoylated CRMP2 peptide aptamer inhibits CaV2.2 trafficking and reverses inflammatory and postoperative pain behaviors. *Pain* **156**, 1247-1264 (2015).
3. W. Ju *et al.*, Suppression of pain-related behavior in two distinct rodent models of peripheral neuropathy by a homopolyarginine-conjugated CRMP2 peptide. *J Neurochem* **124**, 869-879 (2013).
4. A. D. Piekarz *et al.*, CRMP-2 peptide mediated decrease of high and low voltage-activated calcium channels, attenuation of nociceptor excitability, and anti-nociception in a model of AIDS therapy-induced painful peripheral neuropathy. *Mol Pain* **8**, 54 (2012).
5. X. X. Chi *et al.*, Regulation of N-type voltage-gated calcium channels (Cav2.2) and transmitter release by collapsin response mediator protein-2 (CRMP-2) in sensory neurons. *J Cell Sci* **122**, 4351-4362 (2009).
6. D. W. A. Buchan, D. T. Jones, The PSIPRED Protein Analysis Workbench: 20 years on. *Nucleic acids research* **47**, W402-w407 (2019).
7. A. Waterhouse *et al.*, SWISS-MODEL: homology modelling of protein structures and complexes. *Nucleic acids research* **46**, W296-w303 (2018).
8. L. A. Kelley, S. Mezulis, C. M. Yates, M. N. Wass, M. J. Sternberg, The Phyre2 web portal for protein modeling, prediction and analysis. *Nature protocols* **10**, 845-858 (2015).
9. J. Yang *et al.*, The I-TASSER Suite: protein structure and function prediction. *Nature methods* **12**, 7-8 (2015).
10. L. Francois-Moutal *et al.*, Inhibition of the Ubc9 E2 SUMO-conjugating enzyme-CRMP2 interaction decreases NaV1.7 currents and reverses experimental neuropathic pain. *Pain* **159**, 2115-2127 (2018).
11. Y. Xiao *et al.*, Can your protein be sumoylated? A quick summary and important tips to study SUMO-modified proteins. *Anal Biochem* **477**, 95-97 (2015).
12. J. M. Brittain *et al.*, Neuroprotection against traumatic brain injury by a peptide derived from the collapsin response mediator protein 2 (CRMP2). *J Biol Chem* **286**, 37778-37792 (2011).
13. A. M. Pacchioni, J. Vallone, P. F. Worley, P. W. Kalivas, Neuronal pentraxins modulate cocaine-induced neuroadaptations. *J Pharmacol Exp Ther* **328**, 183-192 (2009).
14. A. Moutal *et al.*, SARS-CoV-2 spike protein co-opts VEGF-A/neuropilin-1 receptor signaling to induce analgesia. *Pain* **162**, 243-252 (2021).
15. W. Ju *et al.*, SUMOylation alters CRMP2 regulation of calcium influx in sensory neurons. *Channels (Austin)* **7**, 153-159 (2013).
16. E. J. Akin *et al.*, Building sensory axons: Delivery and distribution of Na_V1.7 channels and effects of inflammatory mediators. *Science Advances* **5**, eaax4755 (2019).
17. E. J. Akin *et al.*, Paclitaxel increases axonal localization and vesicular trafficking of Nav1.7. *Brain* 10.1093/brain/awab113 (2021).
18. T. Fukuoka *et al.*, Comparative study of the distribution of the alpha-subunits of voltage-gated sodium channels in normal and axotomized rat dorsal root ganglion neurons. *J Comp Neurol* **510**, 188-206 (2008).
19. S. D. Dib-Hajj, T. R. Cummins, J. A. Black, S. G. Waxman, Sodium channels in normal and pathological pain. *Annu Rev Neurosci* **33**, 325-347 (2010).
20. D. L. Bennett, A. J. Clark, J. Huang, S. G. Waxman, S. D. Dib-Hajj, The Role of Voltage-Gated Sodium Channels in Pain Signaling. *Physiological reviews* **99**, 1079-1151 (2019).

21. X. Zhang, B. T. Priest, I. Belfer, M. S. Gold, Voltage-gated Na+ currents in human dorsal root ganglion neurons. *eLife* **6**, e23235 (2017).
22. A. M. Rush, M. E. Brau, A. A. Elliott, J. R. Elliott, Electrophysiological properties of sodium current subtypes in small cells from adult rat dorsal root ganglia. *J Physiol* **511 (Pt 3)**, 771-789 (1998).
23. S. Zolotukhin *et al.*, Recombinant adeno-associated virus purification using novel methods improves infectious titer and yield. *Gene Ther* **6**, 973-985 (1999).
24. J. C. Grieger, V. W. Choi, R. J. Samulski, Production and characterization of adeno-associated viral vectors. *Nature Protocols* **1**, 1412-1428 (2006).
25. A. M. Moreno *et al.*, Long-lasting analgesia via targeted in situ repression of Na(V)1.7 in mice. *Sci Transl Med* **13** (2021).
26. I. Decosterd, C. J. Woolf, Spared nerve injury: an animal model of persistent peripheral neuropathic pain. *Pain* **87**, 149-158 (2000).
27. T. L. Yaksh, T. A. Rudy, Chronic catheterization of the spinal subarachnoid space. *Physiol Behav* **17**, 1031-1036 (1976).
28. S. R. Chaplan, F. W. Bach, J. W. Pogrel, J. M. Chung, T. L. Yaksh, Quantitative assessment of tactile allodynia in the rat paw. *J Neurosci Methods* **53**, 55-63 (1994).